THE ROLE OF SPACE WEATHER IN FORMING WATER FROM THE POTENTIAL LUNAR REGOLITH SIMULANT RHYOLITE

A Dissertation
Presented to
The Academic Faculty

by

Aintzane Castarlenas Martinez

In Partial Fulfillment
of the Requirements for the Degree
Master of Science in Chemistry

Georgia Institute of Technology
December 2022

THE ROLE OF SPACE WEATHER IN FORMING WATER FROM THE POTENTIAL LUNAR REGOLITH SIMULANT RHYOLITE

Approved by:

Dr. Thomas Orlando, Advisor
School of Chemistry and Biochemistry
Georgia Institute of Technology

Dr. Brant Jones
School of Chemistry and Biochemistry
Georgia Institute of Technology

Dr. Joshua Kretchmer
School of Chemistry and Biochemistry
Georgia Institute of Technology

Date Approved: 08/26/2022

ACKNOWLEDGEMENTS

First, I would like to thank Dr. Brant Jones, Dr. Sramana Kundu, and Dr. Thomas Orlando for helping and guiding me through this thesis work.

I want to thank Prof. Darby Dyar, Mount Holyoke College, for providing the surrogate samples.

Finally, I want to thank the Radiation Effects on Volatiles and Exploration of Asteroids and Lunar Surfaces (REVEALS) node (80ARC017M0007) of NASA's Solar System Exploration Research Virtual Institute (SSERVI) for financial support.

TABLE OF CONTENTS

LIST OF FIGURES

LIST OF SYMBOLS AND ABBREVIATIONS

TOF	- Time of Flight
RGA	- Residual Gas Analyzer
IR	- Infrared
ESD	- Electron stimulated desorption
EPICS	- Electron and photon induced chemistry on surfaces
PSR	- Permanently shaded regions
RD	- Recombinative desorption
UHV	- Ultra-high vacuum
SEM	- Secondary electron multiplier
LCROSS	- Lunar Crater Observing and Sensing Satellite
E_a	- Activation energy
ANT	- Anorthosite, Norite and Troctolite
UV	- Ultraviolet
M3	-Moon Mineralogy Mapper
MCP	- Microchannel plates

UHV - Ultra-high vacuum

m/z - Atomic mass

H_2O / H_2O^+ - Water

H / H^+ - Hydrogen atom / ion

OH / OH^+ - Hydroxide / Ionized hydroxide

H_2 / H_2^+ - Molecular hydrogen / Ionized molecular hydrogen

H / H^+ - Atomic hydrogen / Hydrogen ion

D / D^+ - Deuterium atom / ion

D_2 / D_2^+ - Molecular deuterium / Ionized molecular deuterium

OD / OD^+ - D- Hydroxide / Ionized D-Hydroxide

D_2O / D_2O^+ - D-Water / Ionized

D_3O / D_3O^+ - Trideuteriooxidanium / ionized

HD / HD^+ - Isotopic specie of hydrogen and deuterium / ionized

HDO / HDO^+ - Isotopic specie of water and deuterium / ionized

SiO_2 - Silicon dioxide

Al_2O_3 - Aluminum oxide

Na_2O - Sodium oxide

CaO - Calcium oxide

FeO - Iron (II) oxide

K_2O - Potassium oxide

SUMMARY

The potential role of the solar wind and space weathering in the formation of water on a lunar surface has been studied by deuteron ion implantation followed by electron bombardment on a silica rich glass surrogate, rhyolite. The electron bombardment stimulates chemistry and leads to water formation and ion desorption. The latter process, electron stimulated desorption (ESD) probes the role of electrons from the solar wind in both producing and desorbing ionic and neutral products. Prolonged electron excitation of deuteron dosed rhyolite samples induces defects on the sample, opening paths for diffusion of molecules to the surface. These experiments lead to the conclusion that solar wind in conjunction with electron bombardment of the lunar soil can generate water and other volatile products such as molecular hydrogen. These processes should be considered when modeling the lunar hydrogen and water pathways or cycles.

1. INTRODUCTION

There has been significant interest regarding the presence of volatile molecules on the lunar surface. Volatile molecules were always considered unstable on the lunar surface because of the high UV solar flux capable of photodissociating these molecules[1,2]. However, a study in 1961 by the Division of Geological sciences at California Institute of Technology, examined the possibility of finding water inside the permanently shaded regions (PSRs) of the moon. In these regions, temperatures can reach 120K[3,4] or lower. This group developed a model to understand the stability of volatiles on the surface using different parameters, including the fraction of lunar surface permanently shaded, and the water evaporation and condensation rate at the cold traps. Evaluating the ratio between water lost by sublimation and trapped within the PSRs lead to the conclusion that water is more stable on the surface of the moon than originally thought, especially in the cold traps[5,6,7].

Many years later, two missions intended to better understand the moon's mineral and molecular composition, confirmed the presence of water on the lunar surface. The Moon Mineralogy Mapper (M3) imaging spectrometer traveled aboard the Chandrayaan-1 spacecraft to orbit the moon[8,9] in 2009. Interpreting the data collected lead to the correlation of H_2O abundance distribution with distance from the equator[10,11,12], spanning latitudes from 10°N to 90°N. The Lunar Crater Observing and Sensing Satellite (LCROSS) which impacted the lunar south pole crater Cabeus, generated a large vapor plume of gas and dust. Within this plume was approximately 2,200 kg of dust, 55 kg of vapor water, and 68 kg of ice, estimating that water constituted 5.6% of the material released by impact[13].

The large volume of ice water detected opened discussions about water delivery methods to the PSR's, supporting the idea of molecular water migration across the lunar surface until landing in a cold trap[10]. Different sources explaining the OH/H_2O optical signature between 2.8 and 3.0 μm in the lunar soil have been suggested, including the implantation of protons from solar wind, at a flux of $4 \cdot 10^{-8}$ $s^{-1}cm^{-2}$ into an overall average depth of 15 nm[15], chemically binding to oxygen within the lunar soil to form hydroxyls. At low latitudes the constant cycle of OH formation and H_2O removal is much more dynamic compared to higher latitudes. The diurnal optical signature of OH/H_2O between 2.8 - 3.0 μm suggest the existence[10] of such a cycle. Over time, the OH concentration in the polar region (75 - 90°) will saturate due to the OH accumulation over loss mechanisms[16] induced by solar wind implantation.

The existence of chemically stable hydroxyls in lunar material has been in the literature for decades. In 1966,[17] experimental evidence of OH formation was obtained after bombarding glass surrogates with protons and approximating the hydroxyl content formed. Hydroxyls are more stable on the moon than water, existing at even the warmest temperatures near the equator[17]. Desorption or removal of hydroxyls occurs by a process called Recombinative Desorption (RD) where a hydroxyl reacts with a neighboring or nearby hydroxyl on the surface forming and desorbing an H_2O molecule[18,19]. Desorbed water molecules continuously hop to new binding sites, undergoing an adsorption/desorption cycle until reaching a cold trap and locking in a binding site. Understanding RD is crucial to determining whether and how the solar wind is involved in water formation on the moon, and potentially explaining the large accumulation of ice water on the poles. It is therefore important to investigate the first step of the process; how

ions are trapped or bound within the lunar grain rims as H^+, H_2^+, -OH, and how solar wind participates on the formation of water. Solar wind can induce H_2 dissociation as well as H diffusion through the lattice defects until they react with oxygen defects to form hydroxyls[10,12,15,16,17]. There are different mechanisms by which H can diffuse though solids, like the diffusion and implantation of hydrogen radicals in locations of broken chemical bonds. Electron bombardment from solar wind can also participate in breaking chemical bonds within the surface grains, creating vacancies within mineral structures known as defects, which can provide a path for proton diffusion. This mechanism requires a significantly low activation energy, typical values are on the order of 0.5-0.7eV depending on the surface[20,21].

A simulation of solar wind implantation using the Monte Carlo method, calculated the dependence of the release of H_2 from the lunar surface on the activation energy of diffusion (E_a)[21]. It concluded that emissive surfaces (E_a = 0.3 eV) release most of the H_2 in less than a lunation (or lunar day), while retentive surfaces (E_a = 0.9 eV) possess more trapping sites with high activation energy, retaining atoms for longer than a lunation. Any surface in between (0.3 eV < E_a < 0.9 eV) is diurnal.

Space weathering can modify the lunar grains by implantation of gasses and pulsed heating, that over time forms thin rims surrounding the lunar grains[28,29]. These amorphous rims generally ranging between 50-250 nm in width[29], can either be compositionally similar or totally distinct to their host grain, some rims also contain nanophase iron. The grains that are constantly exposed to solar wind are known for being defect rich, since defects like vacancies, channels, and crystal loss are distributed around the top 100 nm layer of the grains[30]. The moon has a very weak atmosphere and no global magnetic field,

therefore when it's outside of the earth's magnetosphere, which is 75% of the time, it's exposed to solar wind. Although, only during lunar eclipses the moon is not exposed to solar radiation.

The electron bombardment density[25] measured on the surface during a lunar day is $\sim 3.5\ e^- \cdot cm^{-3}$ with kinetic energies ranging from 0.5 – 10 keV[44]. Research on defects caused by electron bombardment has been conducted for several decades, many studies focused on metal surfaces point defects caused by an electron beam[36], which consists of impurities and vacancies formed on the metal lattice after irradiation. Similarly, defects are generated on lunar soils. A study performed using SiO_2 films[37] concluded that the energy threshold to generate defects on the films was about the same as to ionize 1s core electron from an oxygen atom. Most glasses on the lunar surface have a large SiO_2 molecular composition, therefore defects on lunar soils can be induced by electron bombardment.

Only 10% of the implanted hydrogen particles from the solar wind are desorbed as molecular H_2 [22], this ratio has been calculated using the lunar exosphere density of 1200 H_2 molecules $\cdot cm^{-3}$ and the proton flux from solar wind, providing evidence that lunar soil contains trapped H^+ ions available to form water. RD has been explored by the REVEALS team at Georgia Institute of Technology for the last few years, providing enough experimental evidence that demonstrates that water can be desorbed from the regolith by recombination of two surface hydroxyls, with an activation energy[16,39,40] of $\sim 150\ kJ\ mol^{-1}$.

The activation energies of RD have been studied under vacuum by performing temperature program desorption (TPD) experiments. Experimental results from solar wind

implantation using D_2^+ ions, followed by simulated micrometeorite bombardments[43] (a thermal excitation process) have experimentally demonstrated water production. Solar wind implantation was simulated by irradiation of D_2^+ ions at 5 keV on olivine samples[43], which upon interaction with the surface provoked a bond cleavage, forming a D^+ / D particles each with a kinetic energy of 2.5 keV. Implantation is induced by either an elastic or inelastic transfer process with the surface (15% and 85%, respectively). Elastic transfers lead to the formation silicon oxides, showing evidence of available binding sites on the regolith grains, which subsequently reacted with incoming deuterium to form D-hydroxyl radicals. D-water was then synthesized by RD from laser heating irradiating olivine substrates at temperatures from 10 – 300 K.

1.1 1.1 Hypothesis and Thesis Plan

Water on the moon has been a significant research question for decades, and this project will focus on the study of hydrogen implantation and diffusion through the grain rims induced by electron bombardment, as well as hydroxyl and molecular water formation. Electron bombardment can create defects on regolith grains, opening paths for atomic hydrogen to diffuse at a lower activation energy. During implantation the H atoms are trapped on regolith defects, and H^+ is neutralized by bonding on the lattice to form M-OH or trapped H/H_2. Electron bombardment can lead to enhanced diffusion of the trapped H, and dissociation of chemical bonds or hydroxyl fragmentation, yielding H_2, OH, H_2O formation by the following reactions:

(1) $M\text{-}OH_2 \rightarrow M\text{-}O^+ + H_2$, or $H + H \rightarrow H_2$ (2) M-OH +M-O $\rightarrow$ M-O-M + OH, or H + M-O $\rightarrow$ OH (3) M-OH + H $\rightarrow$ H_2O, or M-OH + M-OH $\rightarrow$ M-O-M + H_2O. The main experimental approach will be divided in two tasks, with the goal of showing evidence of these reactions. The solar wind will be simulated with ionized molecular deuterium and an

electron beam. Tasks 1 will focus on ion implantation and the role of electrons in production of gas phase water on the surface. Tasks 2 will focus on the prolonged effects of electron bombardment, diffusing the trapped H, H_2 molecules and fragmenting the accumulated hydroxyls.

2. EXPERIMENTAL APPROACH

1.2 2.1 Sample simulant of lunar soil

The unconsolidated material that covers the lunar surface is known as regolith; this material is the result of broken lunar rocks from many parts of the moon that preserve signatures of meteorite, solar particles, and cosmic ray bombardment. The lunar surface is divided into Mare and Highland, two regions distinguished by their reflectivity and age. The lunar Highland consists of rocks that belong to the ANT group (Anorthosite, Norite and Troctolite), and it comes from the period or primary crust formation, 4.55–4.2 billion years ago (Ga) [26]. The Mare is formed of a dark basalt considerably younger than the Highland rocks, that was formed by a period of volcanic activity about 4-3 Ga ago[26]. Many grain sizes are displayed in the regolith, and some of them contain glass formed by impact events, that comprise approximately 20-25% of the total lunar regolith[27]. The defects on the grain rims can be caused by electron and ion bombardment from the solar wind[28,29,30]. Samples made from glass surrogates simulate the lunar agglutinates formed by impact events, and their properties are sufficient for the tasks that will be developed in this project. The glass surrogate provided by the Prof. Darby Dyar at Mount Holyoke College shown in Figure 1 is a silica-rich volcanic rock known as rhyolite[31], with a molecular composition of ~75% SiO_2 and ~16% Al_2O_3, and other compounds[31] (2.57% Na_2O, 1.81% CaO, 1.67% FeO, and 1.29 K_2O).

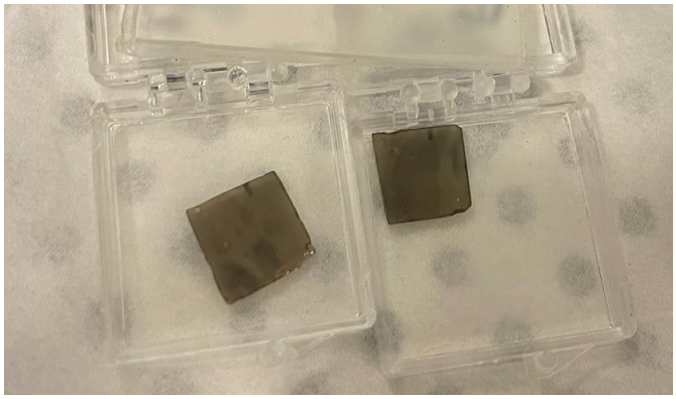

Figure 1: Rhyolite samples. 74.94% SiO_2 and 15.80% Al_2O_3, and other compounds (2.57% Na_2O, 1.81% CaO, 1.67% FeO, and 1.29 K_2O.

1.3 2.2 Experimental apparatus and data collection methods

The Electron and Photon Induced Chemistry on Surfaces (EPICS) lab at Georgia Institute of Technology is equipped with ultra-high vacuum (UHV) chambers, with equipment capable of probing the solar wind hydroxyl and water formation on lunar simulants. The system consists of an ion sputter gun and an electron gun intended to simulate the solar wind plasma, together with a Time-of-Flight (TOF) Mass Spectrometer, and a Residual Mass Analyzer (RGA) for data collection. The UHV chamber is shown in Figure 2.

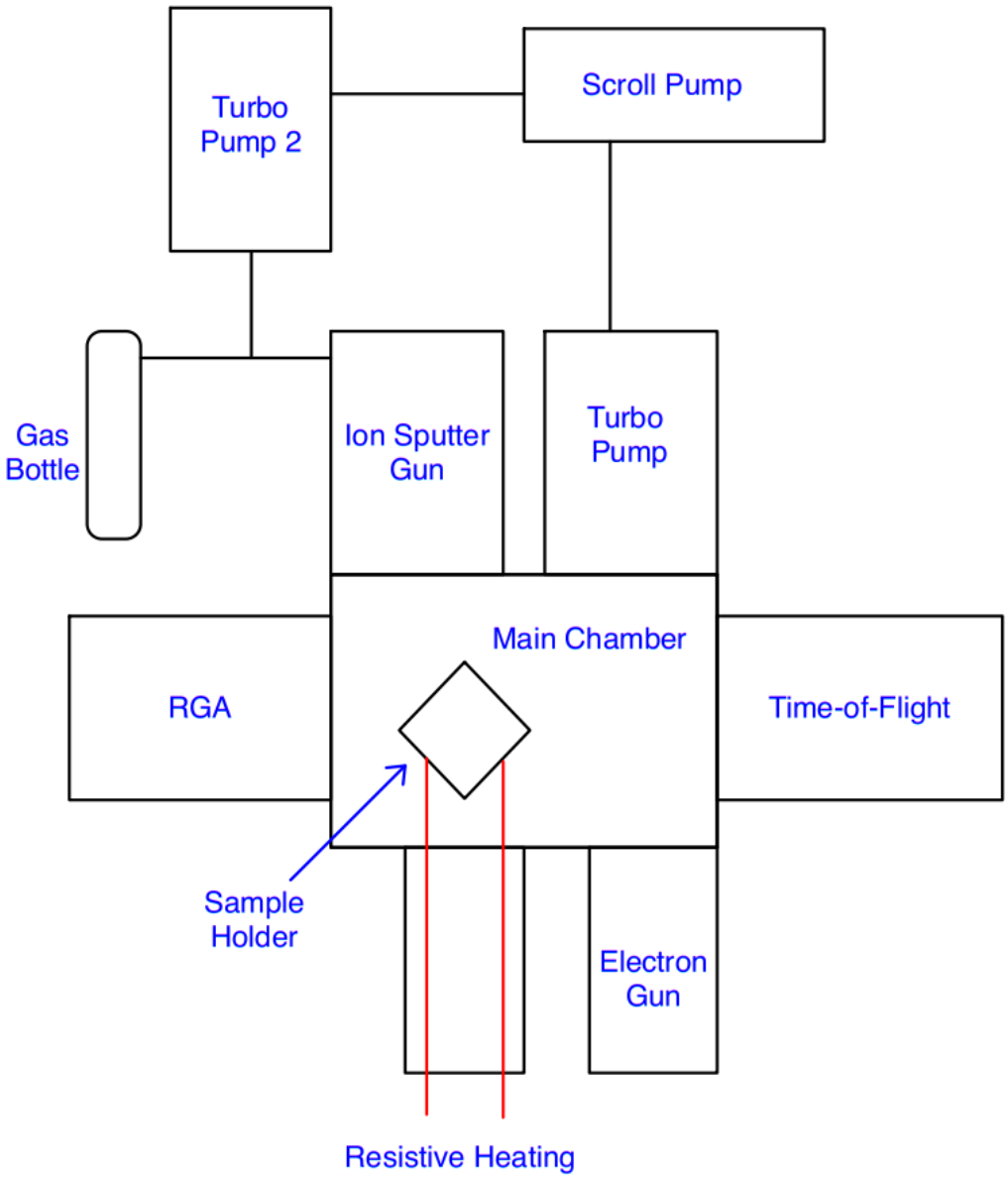

Figure 2: Chamber arrangement. The positions of the electron gun, sample holder and TOF can be adjusted manually. The RGA, turbo pump, and sputter gun are fixed. The sample holder can rotate 360° to allow the sample to face the ongoing radiation method.

The Residual Gas Analyzer (RGA): The RGA is a quadruple mass spectrometer and is typically used to monitor contamination in ultrahigh vacuum systems (UHV), by identifying the partial pressures of gaseous species in the chamber. Gas molecules entering the ionization region are ionized by electron bombardment emitted by a hot cathode, which then are analyzed in the quadrupole fields by measuring the mass to charge valence ratio (m/z) of the ionized particles[23]. The electric charge of the ions can be detected with a faraday cup, or they can enter a secondary electron multiplier (SEM) region for results of higher sensitivity.

The Time-of-flight (TOF) Spectrometer: The TOF spectrometer is designed to capture ions formed and/or released from the sample during electron-impact. The surface molecules are excited by electron bombardment using an electron gun, this method converts the surface chemisorbed particles from a neutral to an excited, either ionic, antibonding, or metastable state. After excitation, energy is then transformed into kinetic energy in a time scale of 10^{-13} seconds[45] allowing for particle motion. Excited molecules then enter the TOF and are detected by the microchannel plates (MCP). The flight time is then used to compute mass resolution.

The Electron Gun: The electron gun uses thermal energy to emit electrons from a cathode, this filament made of tungsten is heated until the free electrons exceed the work function. An electric field is generated between the cathode and the anode, accelerating and converging electrons towards the condensing lens, which are responsible for deflecting the electron beam, a necessary component to facilitate electron bombardment on the full surface, all of which is computer controlled. The energy of electrons used in this project ranges from 100 - 1000 V, generating a flux of electron of about $2 \cdot 10^{13}$ s^{-1} cm^{-2}. Raster scanning methods are continuously used to locate the sample, as well as to assure that ions and products detected by the TOF are solely from the surface of the lunar samples.

Ion sputter gun: The ion sputter gun is necessary to recreate the solar wind ion flux into a vacuum chamber, since it is responsible for implantation of protons on the sample. The gun model purchased from Perkin Elmer is designed to produce a beam of energetic gas ions for sputtering solid surfaces. When electrons are emitted from a tungsten cathode, they collide with gas particles in the ionization region to form an ion beam, which is then deflected by the condensing lens.

As shown in Figure 3, the sputter gun is dosed with molecular D_2 to avoid confusion between nascent surface hydroxyls and the radiolytic species formed. The tubing delivering molecular deuterium from the gas cylinder to the sputter gun, is also provided with a secondary valve connecting the gas lines to a differential pumping system. Scroll pumps, or mechanical pumps, lower the pressure to about 10^{-3} Torr and are necessary for turbo pump operation. Turbo pumps allow the vacuum chamber to reach pressures of approximately 10^{-8} Torr. The differential pumping system consists of a secondary turbo pump functioning separately from the main chamber, and it's used to effectively lower the pressure in the gas lines to match the main chamber conditions. Any remaining water and organics condense on the cryogenic trap, a liquid nitrogen bath in a metal container designed to cool down the gas lines to liquid-nitrogen temperatures via contact with the liquid reservoir. The dosing tube is flexible and therefore molded in a U-shape to fit inside the cooling container, trapping water and volatile organic contaminants more effectively.

The chamber is designed so that the sample is in line-of-sight of the ion and electron guns. The sample holder can be rotated 360° and can move vertically as well. The sample is orientated vertically and held by a metal clip to a thermally controlled mounting plate. The dosing line set up and the differential pumping system is shown in Figure 3. Two high precision rotatory valves are essential to control the gas flow; the first one allows gas to

exit the gas cylinder, and second valve closes the path towards the differential pumping system when deuterium is being dosed. Typical dosing pressures are $2 \cdot 10^{-5}$ Torr.

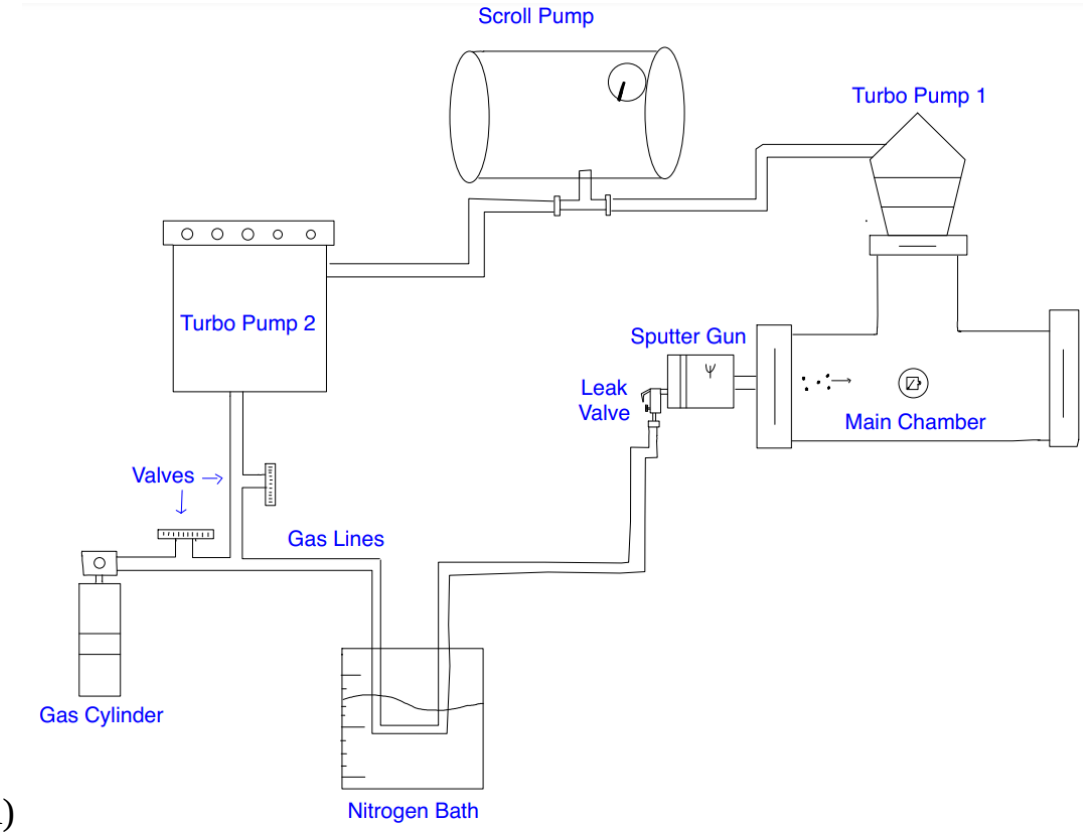

A)

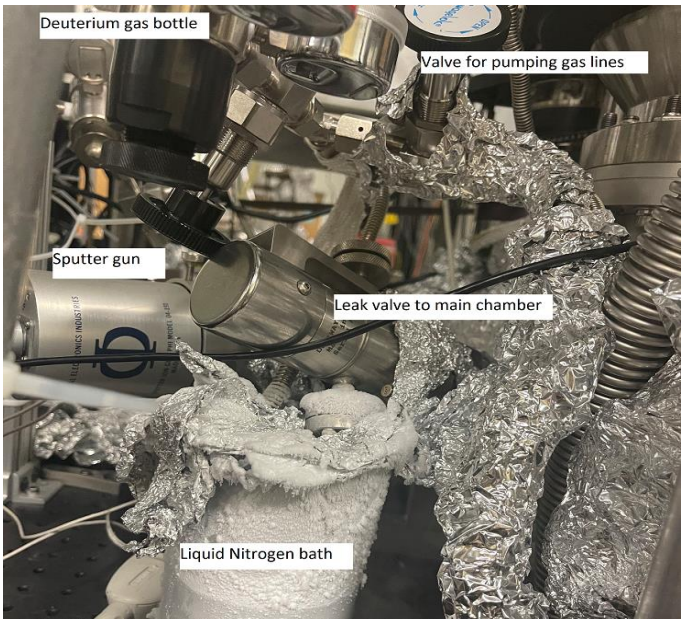

B)

Figure 3: Frame A shows the gas lines set up. Before opening the gas bottle, the valve leading to the turbo pump 2 needs to be closed, to avoid gas waste and possible damage to the turbo pump. Subsequently, when the gas cylinder is opened, deuterium fills the gas lines and the nitrogen bath freezes any water and organics. The leak valve doses the sputter gun with deuterium gas, which is then ionized and directed to the sample. Frame B shows the visual representation of the dosing lines with the liquid nitrogen bath.

3. EXPERIMENTAL CALIBRATION EFFORTS

1.4 3.1 Ion sputter gun calibration

The ion sputter gun is controlled by five variables: Beam voltage, emission current, X-Y coordinates, focus, and raster voltage. The goal is to determine the maximum current intensity by optimizing those variables. A faraday cup placed right under the sample holder is positioned directly in front of the gun, exactly where the sample will be sitting, and it is connected to a picoammeter that reads the ion current. A current of 1.06 μA was reached after gradually modifying the settings with the goal of reaching a maximum current reading. The setting parameters were: 5 kV beam voltage, 40 milliamps emission current, 5.45-2.40 on X-Y coordinates, a zero focus and a raster of 4.4.

The beam voltage generates a potential that accelerates the electrons hitting the gas particles in the ionization region, therefore a higher beam voltage produces more ions of a higher energy. Emission current on the gun is highly stable since it's control by flux regulation, also the gun is operated with a focused beam to get the sharpest spot size. The raster is responsible for the beam size, which according to the manual results in a sputtering area of 1cm x 1cm at a 5cm distance from the source when set at the maximum value on the scale 1 – 10. The sample distance from the beam source was measured to be 11.6 cm, and the samples area around 1cm x 1cm. Therefore, the optimal raster for assuring radiation on the whole surface was 4.4 in the 1 – 10 scale.

The incoming solar radiation carry ions at a flux[15] of $4 \cdot 10^8$ s^{-1} cm^{-2} generating a surface flux of around 0.09 nA, five orders of magnitude smaller than the current detected by the faraday cup. An hour of sputtering with the ion gun corresponds to ~800 days of solar wind radiation on the moon's surface. Although solar wind delivers mostly H^+ions,

the contribution of D^+will be meaningful because their kinetic energy (2.5 keV) falls in in the solar wind range[43] of 1-2 keV per amu (amu of D = 2.014).

1.5 3.2 Electron gun calibration

The electron gun flux profile was calibrated using a more visual method, which includes a deflected electron beam in the X-Y coordinates, and the first lens in the TOF connected to a picoammeter used for charge detection of secondary electrons, which are excited and scattered by the electron beam at 250V. This method is capable of mapping the X-Y coordinates based on the electron charge received, which varies depending on the surface radiated with the electron beam. Mirror images of the sample can be taken using this method. The only two variables in this calibration process are the gun distance from the sample, and the electron beam energy. The step-by-step process consisted of increasing the energy from a starting point of 100V to 1000V, in ten steps. The beam becomes narrower as the energy goes up, which required the distance between the gun and the sample to be increased respectively, from a 2 cm starting point to 9 cm at the highest energy. The distance was increased based on the mirror images taken at each energy, this method was used to keep the beam spot size ratio with the sample relatively constant. The rest of parameters were kept constant throughout the calibration process for an optimal reading, including a source of 2.4V, 4V grid, selected autofocus, and 100V on the 1st anode. All these parameters are controlled by the electron gun controller and selected remotely from the computer software. Electron bombardment can be visually tracked using this method, by plotting mirror images of the sample in the X-Y graph, as it's shown in Figure 4.

The solar wind has an electron flux density[25] of $1.4 \cdot 10^8$ s^{-1} cm^{-2}, again five orders of magnitude smaller than the generated electron beam of $\sim 2.6 \cdot 10^{13}$ s^{-1} cm^{-2}. Electron

bombardment is a non-thermal radiation process, and it is expected to contribute to the ion desorption and the ion diffusion process by forming defects on the surface lattice, opening paths for D diffusion and trapping. The desorption of surface bound species induced by electron excitation is examined by using Electron Stimulated Desorption (ESD). This method has been used since the early 1960's to denote the physical and chemical changes caused in a surface exposed to electron bombardment[34]. In this project, ESD will focus on tracking the stimulated desorption of surface species with a TOF spectrometer, which will scan the D^+, D_2^+, OD^+, D_2O^+, D_3O signals from the surface. The ESD experiment is performed using an electron beam at 250V, inducing instantaneous electron driven scattering reactions on the surface. The ESD experiments directly probe the role of electrons from the solar wind in both producing and desorbing ionic and neutral products. Direct detection of ions with TOF probes the ionic final states whereas other techniques such as quadrupole mass spectrometry or laser detection have to be used for neutral product detection. The yields and products may change with dose and time thus prolonged electron bombardment at 1000 V will be performed to compare the immediate electron-beam effects versus longer irradiation.

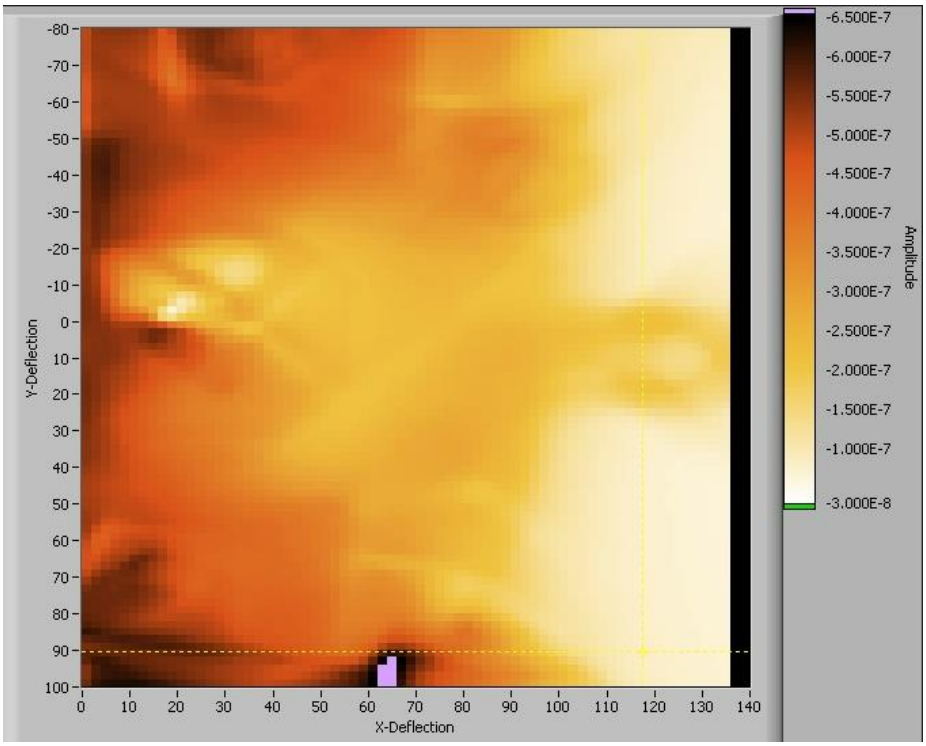

Figure 4: Mirror image of the sample taken with the first electrostatic lens connected to the TOF, and the electron gun at 1000V. The raster allows for the electron deflect the beam in the X-Y coordinates, with a maximum of 150 and a minimum of -150 on both coordinates.

1.6 3.3 Reduction of water in dosing lines using a cryogenic trap

As already described, D_2 is dosed in the ion sputter gun through a stainless-steel tube that is connected to the gas cylinder. The tubing and sputter gun are connected to a differential pumping system that lowers the pressure to similar conditions in the main chamber. Although turbo pumps are capable of reaching low pressures, more specifically around 10^{-8} Torr in this experiment, water and other molecules coating the tubing walls are difficult to remove. A cryogenic trap previously described is used to cool down the tubing walls to ~77K, trapping the water molecules and other organics that could not be removed by standard pumping.

To understand the effectiveness of the cryogenic trap, a preliminary experiment was designed to collect RGA data in the main chamber while D_2 gas was flooded at a pressure of $2 \cdot 10^{-5}$ Torr. The main goal was to observe the gas purity level and a decrease on the water signal when the cryogenic trap was cooling the dosing lines. The ion sputter gun remained turned off throughout the whole experiment since the RGA was actively collecting data, and gas particles were ionized by the RGA cathode.

The main chamber had a pressure of $6 \cdot 10^{-9}$ Torr after pumping over a period of 2 days. First, D_2 gas was flooded into the sputter gun by filling the dosing lines with deuterium from the gas cylinder, subsequently the gas was leaked into the main chamber to a pressure of $2 \cdot 10^{-5}$ Torr, once the desired pressure was reached, an RGA scan was taken. Next step was filling the cryogenic trap with liquid nitrogen and keeping the same gas pressure in the main chamber, after 5 min of cooling down the dosing lines, another RGA scan was collected. Data from the two scans comparing the molecular hydrogen and water abundance in the dosing lines with and without the liquid nitrogen bath is shown in Figures 5 and 6.

3.3.1 RGA Dosing Lines Data

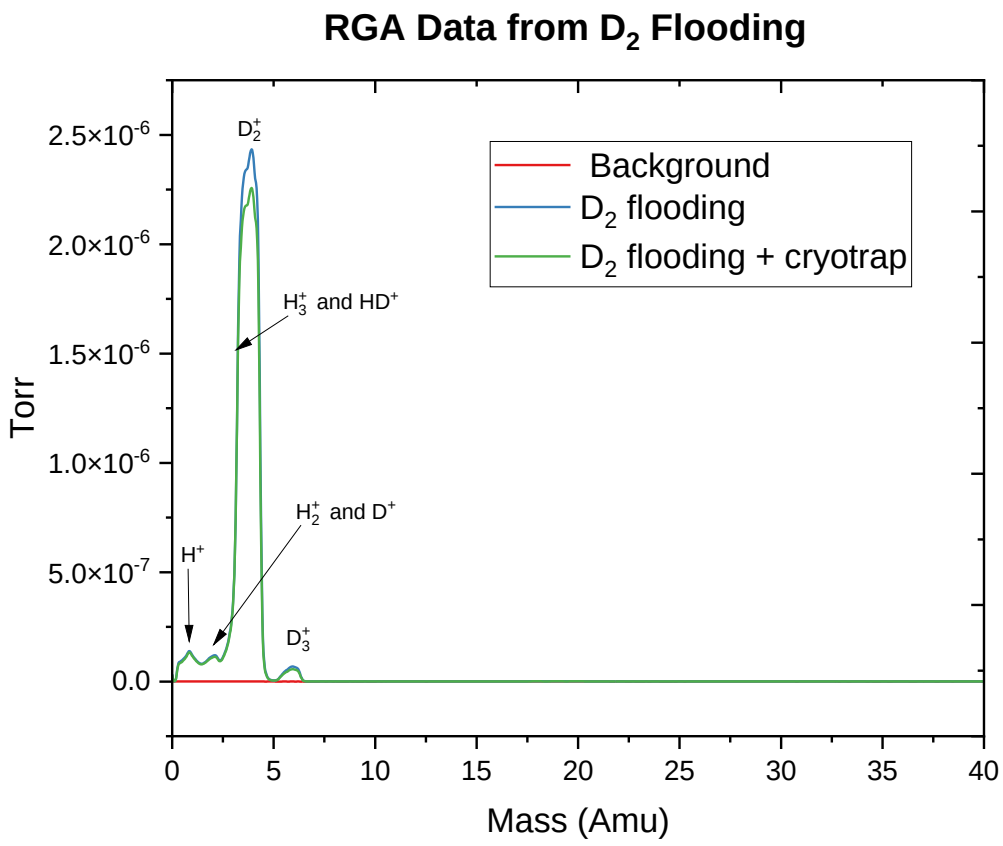

Figure 5: RGA data with an expected peak at m/z = 4 from flooding D_2 in the main chamber. Red line is an RGA scan of the main chamber at $6 \cdot 10^{-9}$ Torr, initial conditions. Blue line is from an RGA scan when D_2 was flooding the chamber at $2 \cdot 10^{-5}$ Torr, and green line includes the cryogenic trap. m/z=1 (H^+), m/z=2 (H_2^+, D^+), m/z = 3 (H_3^+, HD^+), m/z=4 (D_2^+), and m/z=6 D_3^+

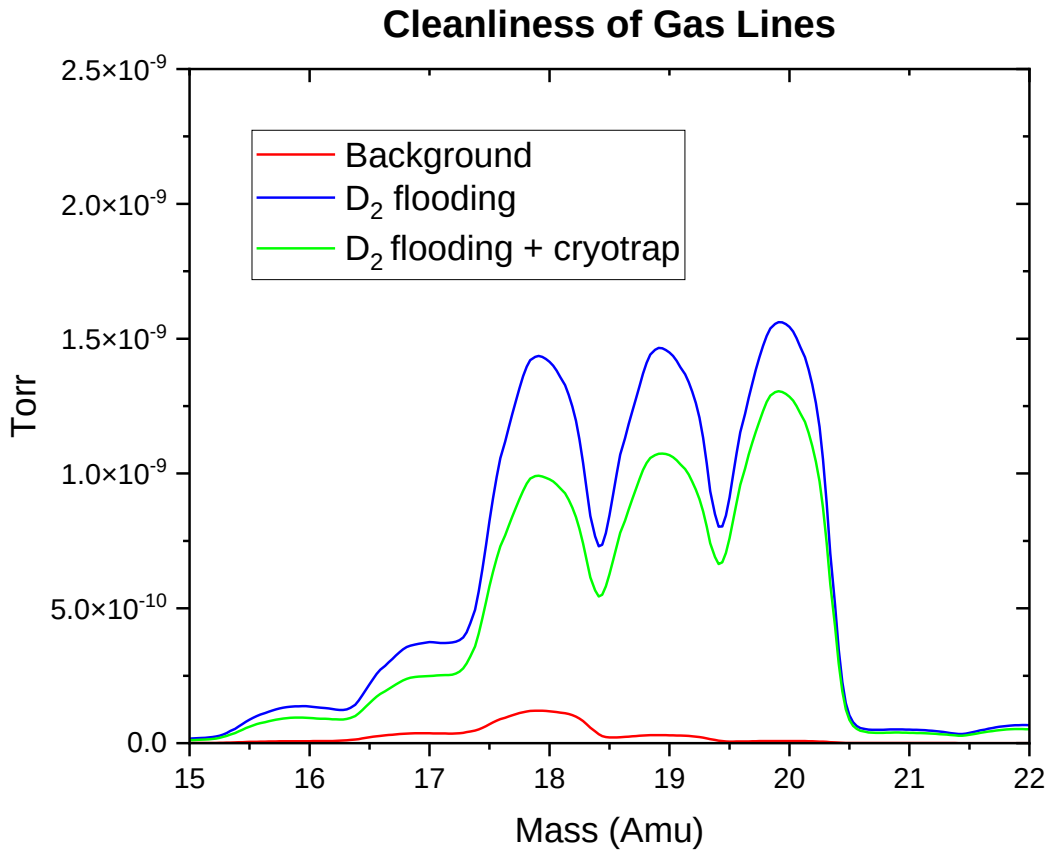

Figure 6: Presence of water molecules in the gas-lines. Visible decrease of water molecules when adding the cryogenic trap. Red line is an RGA scan of the main chamber at $6 \cdot 10^{-9}$ Torr (initial conditions). Blue line is the RGA scan when D_2 was flooding the chamber at $2 \cdot 10^{-5}$ Torr, and green line includes the cryogenic trap. m/z=17 (OH^+), m/z=18 (H_2O^+), m/z=19 (H_3O^+, HDO^+) and m/z=20 (D_2O^+)

Figure 5 shows a dominant peak at m/z = 4, indicating the presence of molecular D_2. There is m/z=1 (H^+), m/z=2 (H_2^+, D^+), m/z = 3 (H_3^+, HD^+), m/z=4 (D_2^+) and m/z=6 (D_3^+) also present in the dosing lines indicating ion molecule reactions in the ionizer. These masses containing some hydrogen are the result from an isotopic exchange in the dosing lines and chamber, and the subsequent ion molecule reactions between the added deuterium and atmospheric gas contaminants primarily in the RGA. The isotopic exchange happens even at low temperatures, and it is induced by the introduction of a heavy isotope in its

molecular form in an environment containing H_2. Though natural abundances of hydrogen and deuterium are 99.9844% and 0.0156% respectively[32], the introduction of D_2 leads to the formation of the ions shown in Figure 5. Masses larger than m/z=40 are not shown in this figure but are present in the sample.

Figure 6 clearly shows three main signals at m/z = 18, 19, 20, emerging after flooding D_2 gas. These masses with low partial pressures ($1.5 \cdot 10^{-9}$ Torr) indicate the presence of background water molecules. Again, isotopic exchange is happening in the dosing lines between the atmospheric water and D_2 gas, forming HDO, D_2O. The incoming flux of these masses needs to be minimized for any experiments dealing with water formation. Adding a cold trap accomplished a decrease of one order of magnitude in the overall signal, but it did not lead to total removal of water. The rate at which these molecules hit and contaminate the sample depends on their partial pressure. It's established that at 760 Torr, $2.9 \cdot 10^{23}$ particles hit an area of 1 cm^2 per second. At the experimental pressure of $2 \cdot 10^{-5}$ Torr, every second $\sim 10^{10}$ particles with masses 18, 19, and 20 are hitting the sample (300 K).

Effectively reducing the water presence could also be accomplished by baking the chamber more aggressively over a period of a week and extending the dosing lines to allow for the addition of more surface area under cryogenic temperatures. This approach will be implemented in future projects, although the total removal of atmospheric water contamination can only be accomplished using a mass-selected ion beam, generated by the ion gun/Wein filter combination as discussed in Chapter 6. This apparatus operates with two differential pumping systems that ensure the removal of any unwanted neutrals and ions. Upcoming projects will use the solar wind chamber at the EPICS lab, which is equipped with a mass-selected ion-beam.

4. TASK 1: STUDY OF ION IMPLANTATION ON LUNAR SIMULANTS

The solar wind consists of a continuous flow of ions traveling through space at 400 km/s, containing mostly H^+ ions[35]. As mentioned earlier, the flux of protons incoming from the sun is greater than the lunar exosphere density, which means that vast majority of particles are implanted into the lunar soil. This chapter explores how incoming ions from simulated solar wind interact with the rhyolite samples and the effects of instantaneous electron bombardment.

The experimental approach has been described in Chapter 2. A rhyolite sample was placed in the chamber using the sample holder, then the main chamber and dosing lines were pumped down over 24 h. The solar wind simulation was generated with the previously calibrated ion sputtering gun for a duration of 1 h, corresponding to ~800 lunar days of solar wind exposure on the equator. The established raster deflected the beam radiating 1 cm^2 of surface area, with a current of 1.06 μA. The main chamber had a staring pressure of $1.7 \cdot 10^{-8}$ Torr, and then D_2^+ ions were dosed at a pressure of $2 \cdot 10^{-5}$ Torr. ESD measurements are taken with a pulsed 250 eV electron beam at 1 hertz. This supplied a total dose of $\sim 7.5 \cdot 10^{15}$ electrons cm^{-2}. The cryogenic trap was actively being refilled every 15-20 min, partially trapping some water and organic contaminants. The surface composition was examined using a TOF spectrometer, taking scans before and after radiation. TOF mass spectrometry results from background and after deuterium ion and irradiation are shown in Figure 7.

1.7 4.1 Ion implantation and electron bombardment on rhyolite samples

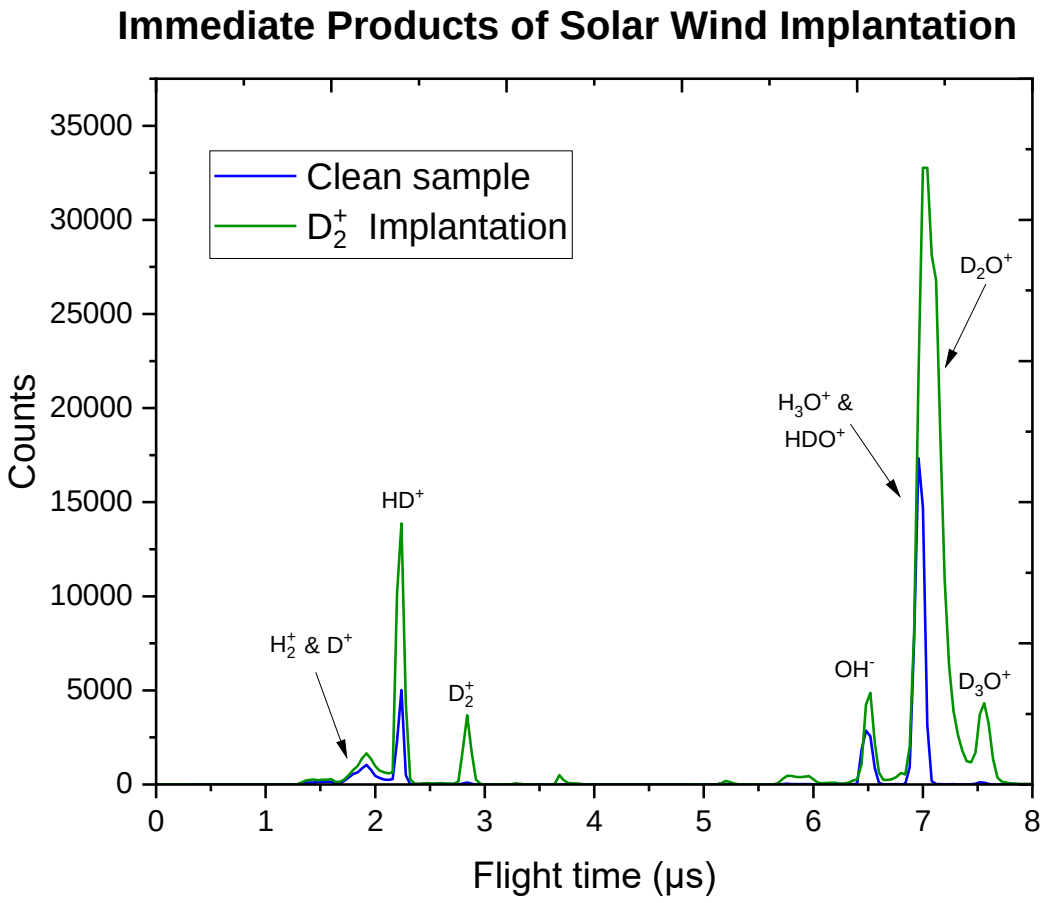

Figure 7: Ions produced and removed from a rhyolite sample during an instantaneous electron bombardment. Data taken with a TOF spectrometer before and after dosing with the deuterium ions using a sputter gun. Clearly increasing signals on peaks m/z = 2 (H_2^+, D^+), m/z = 3 (HD^+) and m/z = 4 (D_2^+) due to D_2^+ dosing. There is also m/z = 17 (OH^+), 18 (OD^+, H_2O^+), 19 (HDO^+, H_3O^+) 20 (D_2O^+) and 22 (D_3O^+). Mass 19/20 cannot be resolved due to a similar flight time and the large signal detected.

Measurements taken with the time of flight 10 minutes after solar wind simulation, show the formation and removal of several hydrogen and water group ions. Preliminary calibration assigns the peaks on low masses as m/z = 2 (H_2^+, D^+), m/z = 3 (HD^+) and m/z = 4 (D_2^+), although hydrogen and water products will be neglected as they are nascent molecules on the sample. The increasing signal on m/z = 3 indicates formation of HD^+, from either incoming D^+ which may react with the nascent hydroxyls on the rhyolite sample, or from the present isotopic exchanged HD molecules in the dosing lines. The TOF peak m/z=2 (D^+) shows evidence of the bond cleavage from M-OD sites.

Most importantly, the formation of D-water molecules is visible on the increasing peaks with at m/z = 19 (HDO^+), 20 (D_2O^+) and 22 (D_3O^+). These water group ions show the important role of both proton and electron bombardment on the non-thermal formation of water. This has not been demonstrated before. The reaction network of solely the D_2^+ implantation process is shown in Figure 8, while the non-thermal excitation reactions induced by electron bombardment are shown in Figure 9.

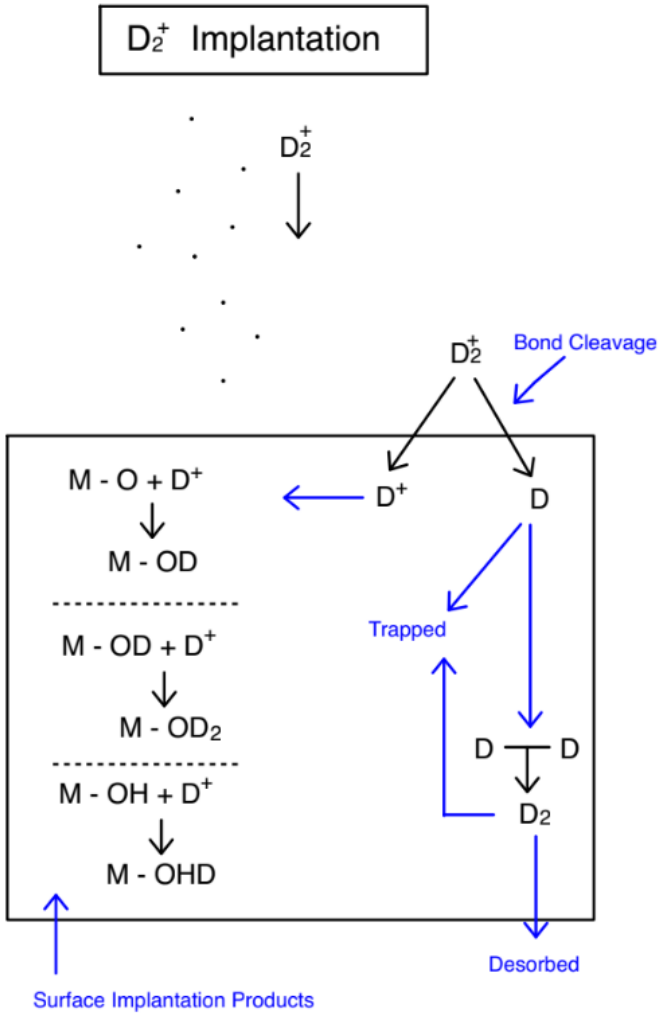

Figure 8: Incoming D_2^+ ions from solar wind break into D/D^+ particles by inelastic collision upon contact with the surface, forming M-OD and M-OHD sites within the rims. M-OH are present in the sample before irradiation (nascent hydroxyls) or can also form by the H_2 present in the dosing lines. Elastic collisions form new surface oxides which then generate more M-OD sites

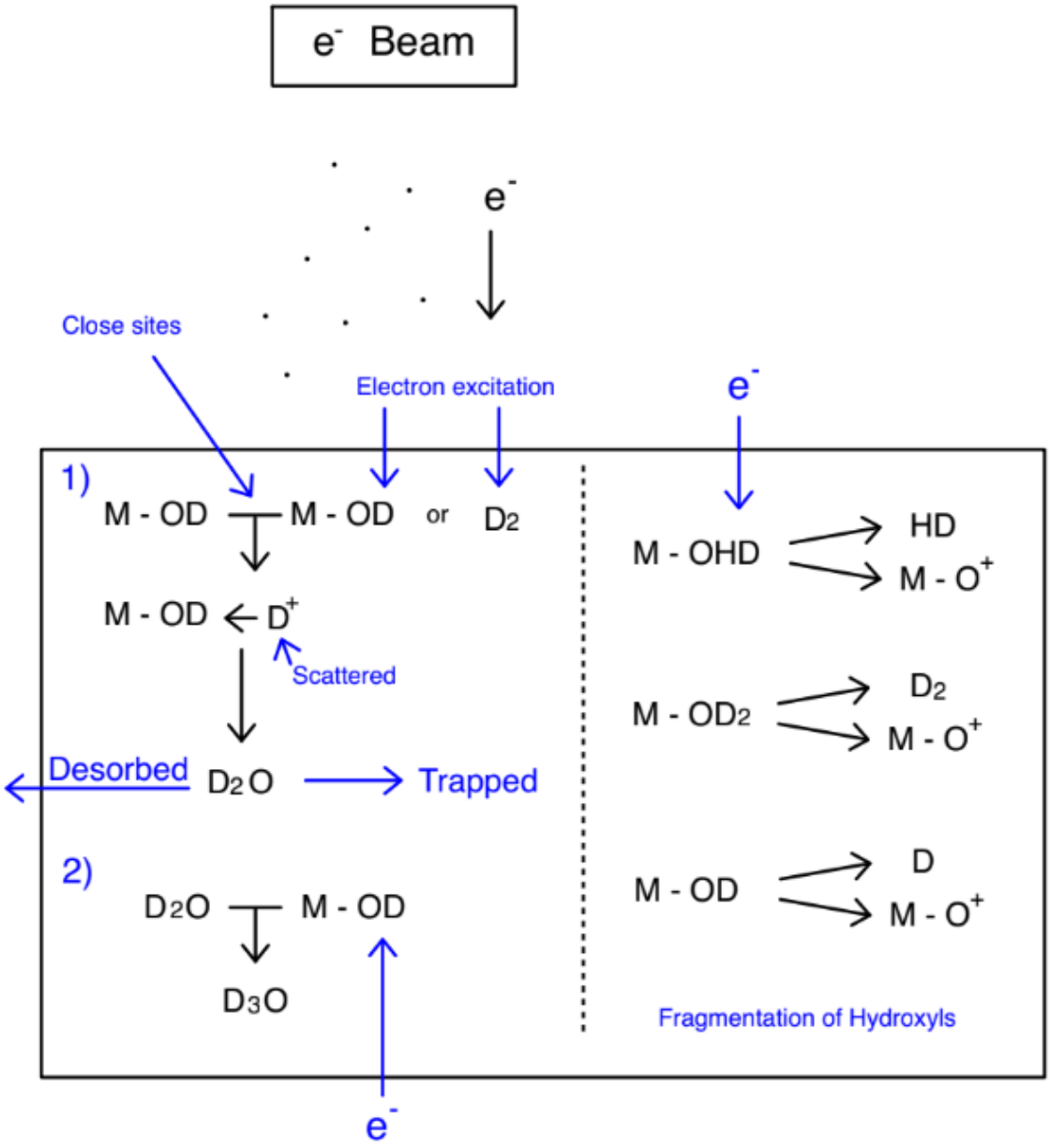

Figure 9: Diagram of the reaction network induced by immediate effects of an electron beam with energy 250V. Reactive D^+ species are formed by electron excitation from a D-hydroxyl group or trapped D_2. These reactive species have a high kinetic energy, which can scatter and form water if they are close to another M-OD site. Another excited D^+ ion interaction with the D_2O^+ molecules will make D_3O^+. Also, an electron can break an M-OHD bond releasing m/z=3 (HD^+), same hydroxyl fragmentation forms m/z=2,4 (D^+/D_2^+). Reactive D radicals in can also occur MOD + D →M + D_2O. The ESD work looks primarily at what occurs right at the surface. The prolonged electron irradiation experiments yields some additional information on subsurface processes such as diffusion.

5. TASK 2: STUDY OF PROLONGED ELECTRON BOMBARDMENT EFFECTS ON RHYOLITE AFTER ION IMPLANTATION

The instantaneous effect of electron bombardment on the formation of water group ions was clearly shown in Figure 7. Electrons from solar wind are actively bombarding the moon surface and they can cause the formation of defects on/in SiO_2 via non-thermal excitation process, creating vacancies on the lattice and allowing for ion diffusions at a lower activation energy cost. When protons diffuse through the surface, they can create new hydroxyls in the lunar soil, and these must be involved in water formation

Task 1 demonstrated the instantaneous effect of electron bombardment however, diffusion and radiation induced diffusion processes can occur on longer time scales. To investigate this, the sample is first dosed with deuterium ions following the same experimental approach in task 1. Subsequently, the irradiated sample with implanted deuterium is bombarded with electrons for a longer duration. The experimental approach and calibration have been previously discussed in earlier chapters. The rhyolite sample was first placed in the main chamber using the sample holder. The chamber pressure was pumped down over a period of 24 h, reaching a pressure of $1.5 \cdot 10^{-8}$ Torr. The same procedure mentioned in task 1 was followed to irradiate the sample with D_2^+ ions at a distance of 9 cm from the sample, followed with electron beam irradiation at 1000 V for two hours of electron bombardment with an emission current of 4-5μA. This simulates a total of ~1500 days of electron bombardment by solar wind on the moon at the equator, supplying a total dose of $\sim 1.8 \cdot 10^{17}$ electrons.

Data was collected with a TOF spectrometer. The first scan was taken after 1h of ion implantation using the same parameters as in chapter 4, and the final scan was taken after the 2h of electron bombardment. The combinations of protons and electrons compose more than 99% of the solar wind. The extended electron bombardment effects on an ion rich surface are shown in Figure 10.

1.8 5.1 Electron bombarding on rhyolite samples

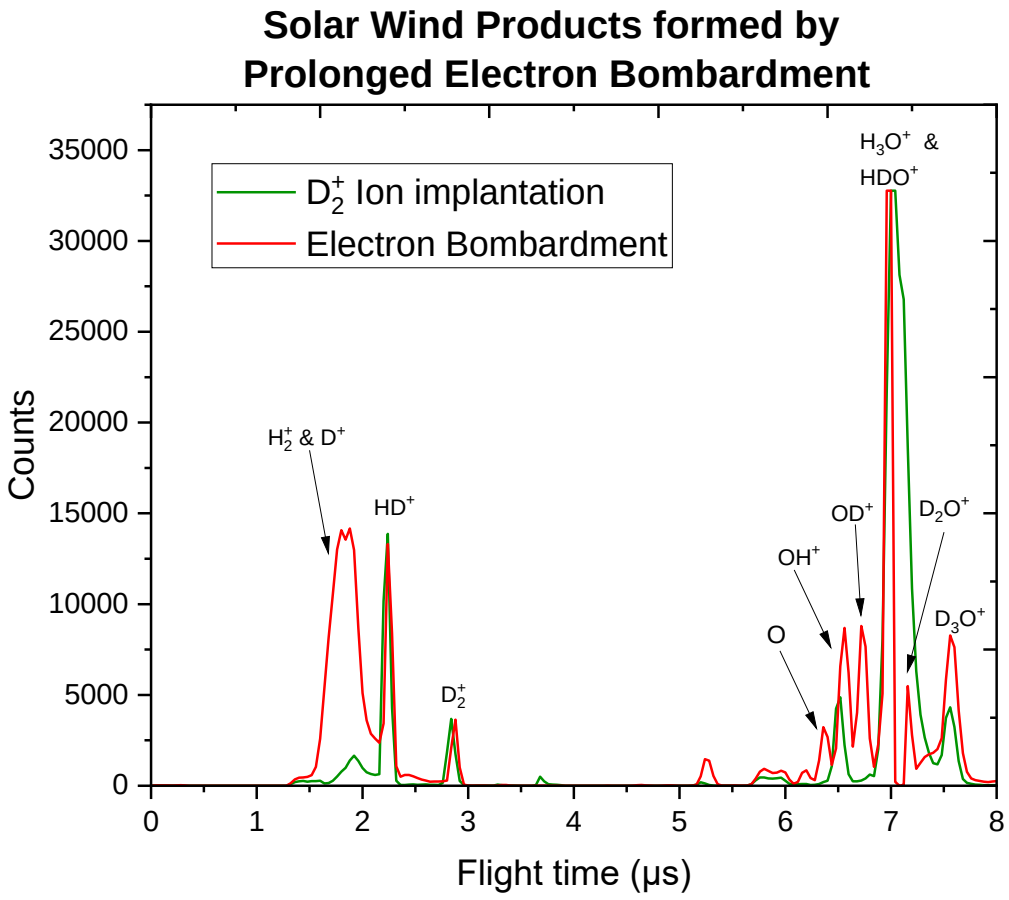

Figure 10: Data collected after 2h of electron bombardment on a deuterium ion dosed rhyolite surface (red line). Signal of m/z = 3 (HD^+), 4 (D_2^+) stay constant after electron bombardment, with a large increase of m/z=2 (H_2^+ and D^+) due to dissociation of trapped D_2 molecules or D_2O, also from trapped H_2 molecules diffusing to the surface. New peaks formed at m/z = 16 (O^+), 18 (OD^+), and significant increase on water peaks m/z = 19 (HDO^+), 20 (D_2O^+) and 22 (D_3O^+).

The peaks formed on figure 10 are the result from a long-term exposure to the non-thermal excitation process. The three main peaks observed are m/z = 18, 20, 22 which indicate the new formation of OD^+ and increased signal of D_3O^+ and D_2O^+ relative to the instantaneous measurement. This is a significant result which implies that stimulated diffusion and products correlated with electron bombardment accumulate over time. For example, the diffusion of OD, D and D^+ and ions to the surface induced by electron bombardment, allow for the production of reactive scattering sites on the surface forming M - OD, M – OD_2 and possibly M – D_2O^+. The continuous non-thermal formation of D^+, from trapped D_2 or M-OD sites, and the stimulated diffusion of OD, D, D^+, all contribute to the increased signals at m/z = 18, 19, 20 and 22. The clearest signature for the role of deuterium implantation followed by electron bombardment is the increased signal of D_3O. The large increase on m/z = 2 may be due to residual D_2, although after 2h of electron bombardment, the chamber pressure was lower than the starting pressure, and an RGA scan indicated no presence of residual D_2. The ESD of D^+ is one of the expected primary ESD channel, it most likely indicates a larger number of terminal M-OD sites, and dissociation of D_2 trapped in the rims. The non-thermal excitation process might also participate in the formation of H_3O^+ ions which can be due to the increased amount of background H_2O present after prolonged electron beam exposure. This is also typically a dominant ESD product from metal oxides containing chemisorbed water[15,16]. Electron bombardment can also induce fragmentation of nascent hydroxyls increasing the oxygen signal observed on figure 10. Overall, there is likely neutral D_2 present, not shown in these measurements, and the electron beam will create non-thermal reactive D atoms and D^+ which can form

OD, D_2O^+ and D_3O^+. The reaction network of prolonged electron bombardment is shown in Figure 11.

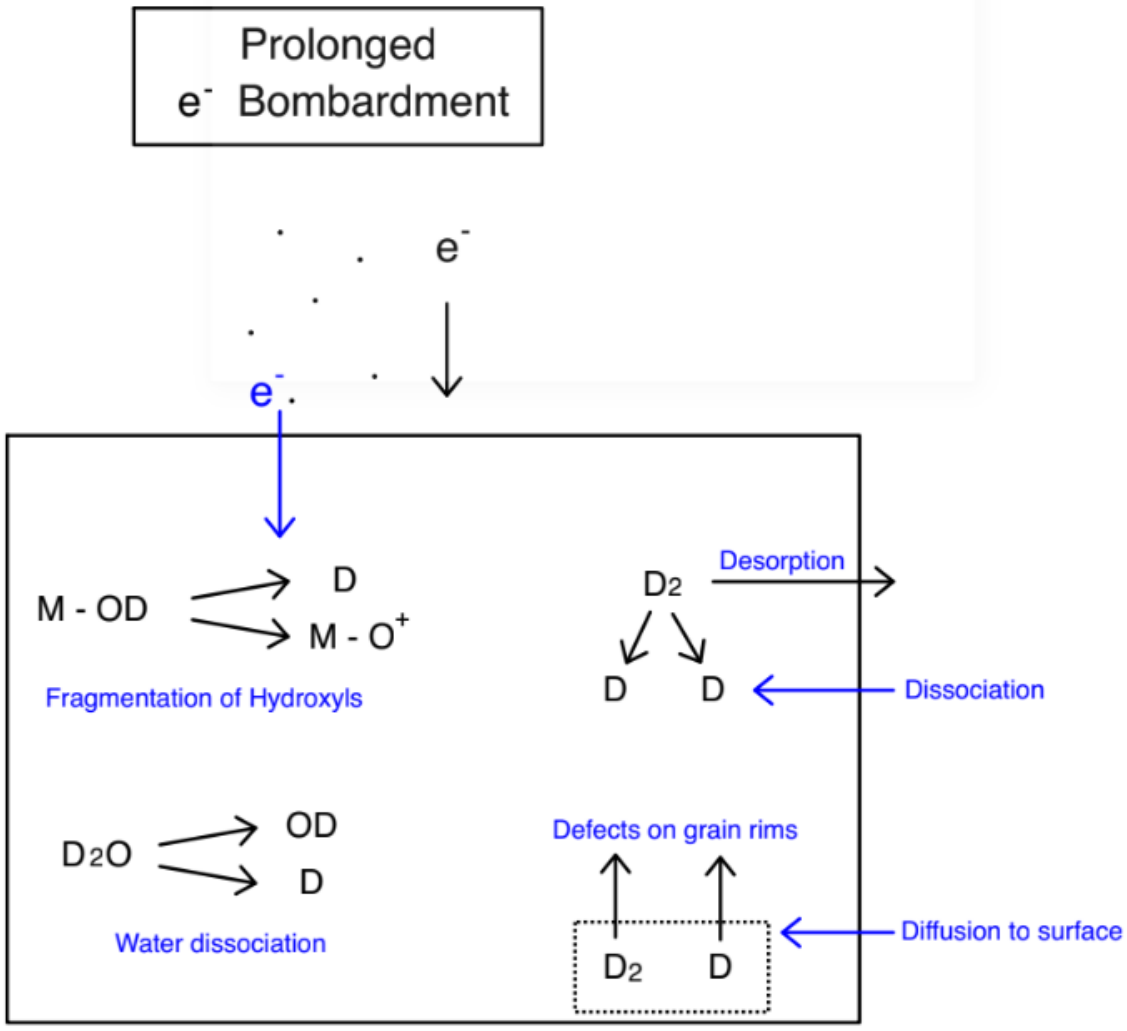

Figure 11: Diagram of new reactions based on results from figure 9, assuming that reactions om Figure 10 are still present but not shown on the diagram. Prolonged electron bombardment induce the continuous fragmentation of D-hydroxyls and dissociation of trapped D_2, forming reactive scattering species, that contribute to the formation of m/z=18,19,20,22. The electron bombardment also participated in the formation of defects on the rims, opening paths for stimulated diffusion of D, D_2. Dissociation of D_2O also contributes to OD signal (m/z = 18). Formation of D_2O and D_3O is continuously induced by electron excitation like shown in Figure 10.

6. FUTURE IMPLICANTIONS USING A MASS SELECTED ION BEAM

As already stated, the use of a differentially pumped ion-beam is likely a better surrogate of the solar wind. Atmospheric contamination was minimized using the cryotraping techniques and the use of deuterium. However, there may be isotope effects in the cross sections for stimulated dissociation of D_2, M-OD, etc. and the subsequent reactive scattering cross sections leading to water formation. Thus, making quantitative assessments of the absolute role of electrons in the formation of water difficult. Therefore, it's necessary to use clean H^+ and D^+ ion beams to minimize the water presence in any experiment dealing with water formation and to allow absolute measurements.

The most effective instrument to allow this is the mass-selected ion beam. The EPICS lab is equipped with a mass-selected ion beam that consists of a Wein filter attached to an ion gun operating with two differential pumping systems. The Wein filter generates a magnetic field that can be adjusted to select particles based on their velocity (mass), allowing solely the particles of interest to enter the main chamber as a beam of ions. The unwanted particles are deviated by the magnetic field and sent through the differential pumping.

Future water formation experiments will be performed in the solar wind chamber that contains a mass selected ion beam. The UHV system shown in Figure 12 is ostensibly the same, however, the TOF will be placed on a vertical flange that can move up and down, facing the sample directly. The mass selected ion beam will also be positions at a 45° angle relative to the surface normal. The ion beam will be generated using either hydrogen and or deuterium gas. The sample holder will consist of a copper flag attached to a linear stage

connected to a cryohead capable of reaching liquid nitrogen temperatures, also equipped with resistive heating and a thermocouple for temperature control. This will allow temperature-controlled reactions and isothermal measurements necessary to extract kinetic parameters. The experimental approach will be repeated ranging from cold trap temperatures (60K) to near equator surface temperatures (450K).

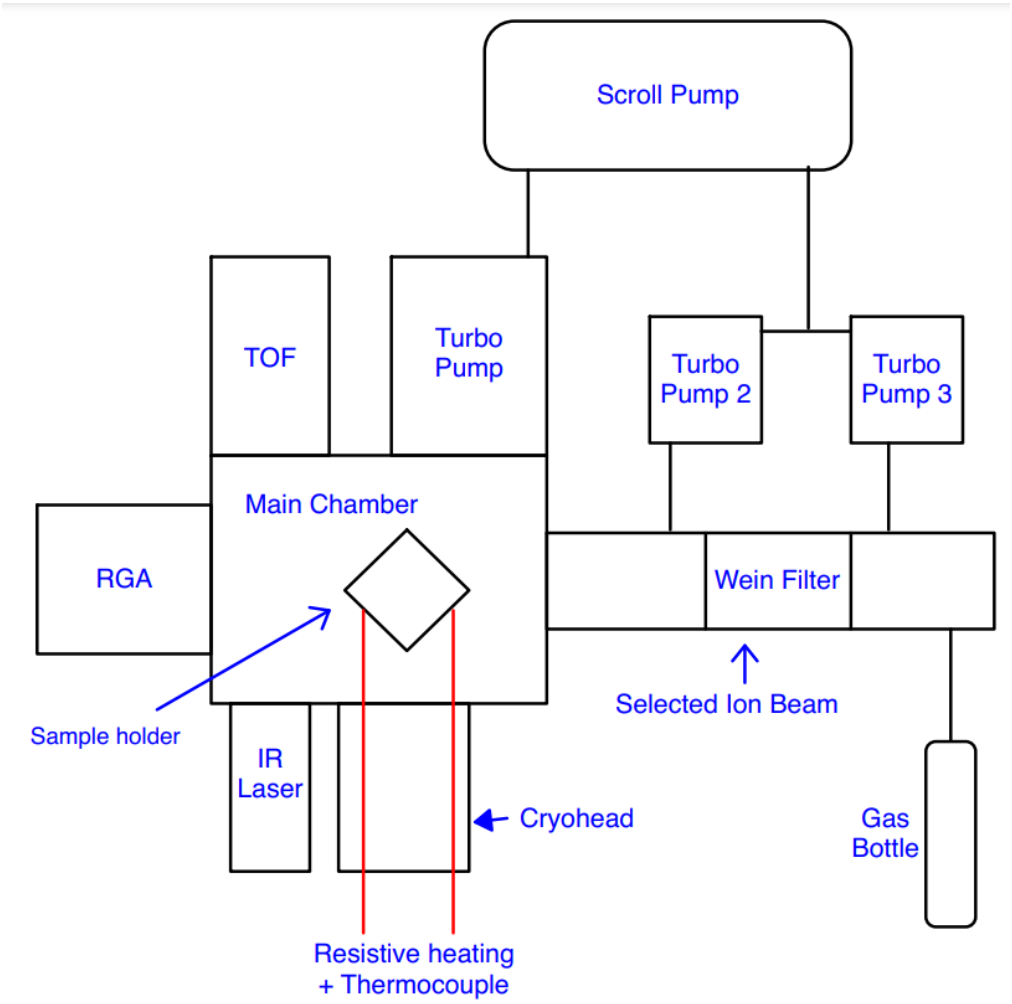

Figure 12: Solar wind UHV chamber distribution. A cryohead attached to a sample holder can vary the sample temperature from $\sim 60 - 450$ K. Selected ion beam used for solar wind simulation, attached to two differential pumping systems to minimize atmospheric gas contamination. IR laser generate high energy impacts simulating micrometeorite impacts. Data is collected with an RGA and TOF spectrometer in-situ. Gas bottle doses molecular Deuterium into the first region of the ion gun.

7. CONCLUSIONS

The role of solar wind and space weathering on the formation of volatiles, such as water and molecular hydrogen has been studied usin implantation of D_2^+ into rhyolite, a lunar simulant, followed by electron irradiation. The ion implantation forms M-OD sites and possibly trapped D, D_2 molecules within the rhyolite sample. Implantation induced formation of M-OD sites was also observed from the electron beam irradiation studies since this causes the non-thermal removal of protons and D^+ by a process known as electron-stimulated desorption (ESD). The ESD results also show clear peaks at m/z = 19, 20, 22, which are likely dominated by HDO^+, D_2O^+ and D_3O^+. These serve as signatures for the formation and release of water from the rhyolite surface. The prolonged electron bombardment studies give further evidence of this process and also indicated evidence that diffusion and transport of D and M-OD to the surface occurs during electron irradiation. This may be due to defect production, radiation induced diffusion and direct dissociation of trap D_2. Since the ESD results increased the m/z = 2 signal by a significant amount after 2h of electron bombardment, fragmentation of M-OD is likely.

Overall, the experimental results show that electron bombardment synergistic with or following solar wind ion implantation can participate in the formation of water from proton irradiated rhyolite samples. The instantaneous effects of electron irradiation yielded D_2O and D_3O, formed by D scattering sites on the surface reacting with implanted M-OD sites. However, only the prolonged bombardment by electron induces diffusion to the surface of OD, D, D_2 through grain defects. Dissociation from the trapped D_2 molecules in the grain defects increased the m/z = 2 significantly after long electron irradiation exposure as well

as M-OD fragmentation. The continuous diffusion of OD, D, D_2 to the surface, as well as the continuous hydroxyl fragmentation on the surface, generate D scattering sites that participate in the formation of HDO^+, D_2O^+, and D_3O^+, as seen on the increasing m/z=19, 20, 22 peaks.

These experiments lead to the conclusion that solar wind in conjunction with electron bombardment of the lunar soil can generate water and other volatile products such as molecular hydrogen. The absolute cross sections have not been measured but the results imply that these processes should be considered when modeling solar wind space weathering of unprotected and unshielded airless bodies such as the moon and asteroids. These synergistic solar proton and electron interactions with space weather surfaces are likely critical to fully understanding the lunar hydrogen and water pathways or cycles.

REFERENCES

[1] Kuiper, G. P., Planetary atmospheres and their origin, in The Atmosphere of the Earth and Planets, revised edition, edited by G. P. Kuiper, University of Chicago Press, Chicago, p. 367, 1952.

[2] Opik, E. J., and S. F. Singer, Escape of gases from the moon, J. Geophys. Research, 65, 3065-3070, 1960.

[3] Watson, K., Murray, B. C., and Brown, H. (1961), The behavior of volatiles on the lunar surface, J. Geophys. Res., 66(9), 3033– 3045.

[4] Watson, K., B. Murray, and Harrison Brown, On the possible presence of ice on the moon, J. Geophys. Research, 66, 1598-1600, 1961.

[5] H. C. Urey, The Planets: Their Origin and Development (Yale Univ. Press, New Haven, CT, 1952).

[6] Arnold J. R., J. Geophys. Res. 84, 5659 (1979).

[7] Crider D. H., Vondrak R. R., Adv. Space Res. 30, 1869 (2002).

[8] Green, R. O., et al. (2011), The Moon Mineralogy Mapper (M3) imaging spectrometer for lunar science: Instrument description, calibration, on-orbit measurements, science data calibration and on-orbit validation, J. Geophys. Res., 116, E00G19, doi:10.1029/2011JE003797.

[9] Chandrayan-1, India's first Mission to the moon. Page 52.

[10] C. M. PIETERS J. N. GOSWAMIR. N. CLARKM. ANNADURAIJ. BOARDMAN. Character and Spatial Distribution of OH/H2O on the Surface of the Moon Seen by M3 on Chandrayaan-1. SCIENCE, Vol 326, Issue 5952. (2009)

[11] J. M. Sunshine et al., Science 326, 565 (2009)

[12] Clark, R. N. (2009). Detection of Adsorbed Water and Hydroxyl on the Moon. Science, 326(5952), 562–564.

[13] A. Colaprete, P. Schultz, J. Heldmann, D. Wooden, M. Shirley, K. Ennico, B. Hermalyn, W. Marshall, A. Ricco, R.C. Elphic, D. Goldstein, D. Summy, G.D. Bart, E. Asphaug, D. Korycansky, D. Landis, L. Sollitt, Detection of water in the LCROSS Ejecta Plume Science, 330 (2010).

[14] Kristen M. Luchsinger, Nancy J. Chanover, Paul D. Strycker, Water within a permanently shadowed lunar crater: Further LCROSS modeling and analysis, Icarus, Volume 354, 2021.

[15] Bennett, C. J., Pirim, C., & Orlando, T. M. (2013). Space-weathering of solar system bodies: A laboratory perspective. Chemical Reviews, 113(12), 9086– 9150.

[16] Jones, B. M., Aleksandrov, A., Hibbitts, K., Dyar, M. D., & Orlando, T. M. (2018). Solar wind-induced water cycle on the Moon. Geophysical Research Letters, 45, 10,959– 10,967.

[17] Zeller, E. J., Ronca, L. B., & Levy, P. (1966). Proton-induced hydroxyl formation on the lunar surface. Journal of Geophysical Research, 71(20), 4855– 4860.

[18] Poston, M. J., G. A. Grieves, A. B. Aleksandrov, C. A. Hibbitts, M. D. Dyar, and T. M. Orlando (2013), Water interactions with micronized lunar surrogates JSC-1A and albite under ultra-high vacuum with application to lunar observations, J. Geophys. Res. Planets, 118, 105– 115

[19] Hibbitts, C. A., G. A. Grieves, M. J. Poston, M. D. Dyar, A. B. Alexandrov, M. A. Johnson, and T. M. Orlando (2011), Thermal stability of water and hydroxyl on the surface of the Moon from temperature-programmed desorption measurements of lunar analog materials, Icarus, 213(1), 64– 72.

[20] Starukhina, L. V. (2006). Polar regions of the Moon as a potential repository of solar-wind implanted gases. Advances in Space Research, 37(1), 50– 58.

[21] Tucker, O. J., Farrell, W. M., Killen, R. M., & Hurley, D. M. (2019). Solar wind implantation into the lunar regolith: Monte Carlo simulations of H retention in a surface with defects and the H2 exosphere. Journal of Geophysical Research: Planets, 124, 278– 293.

[22] Hurley, D. M., Cook, J. C., Retherford, K. D., Greathouse, T. K., Glad-stone, G. R., Mandt, K., Grava, C., Kaufmann, D., Hendrix, A. R., Feldman, P. D., Pryo, W., Stickle, A., Cahill, J., Killen, R. M., & Stern, S. A. (2016). Contributions of the solar wind and micro-meteoroids to molecular hydrogen in the lunar exosphere. Icarus, 283, 31– 37.

[23] The vacuum Techology Book, Volume 2. Pfeiffer.

[24] Time-of-Flight Spectrometry. Agilent Technologies, 2011. 5990-9207EN.

[25] Halekas, J. S., Bale, S. D., Mitchell, D. L., and Lin, R. P. (2005), Electrons and magnetic fields in the lunar plasma wake, J. Geophys. Res., 110, A07222, doi:10.1029/2004JA010991. Table 1.

[26] Arden L. Albee, Lunar Rocks, Editor(s): Robert A. Meyers, Encyclopedia of Physical Science and Technology (Third Edition), Academic Press, 2003, Pages 825-837, ISBN 9780122274107

[27] Okrusch, M., Frimmel, H.E. (2020). Lunar Rocks and the Moon's Interior. In: Mineralogy. Springer Textbooks in Earth Sciences, Geography and Environment. Springer, Berlin, Heidelberg.

[28] Lindsay P. Keller, David S. McKay,The nature and origin of rims on lunar soil grains, Geochimica et Cosmochimica Acta, Volume 61, Issue 11, 1997, Pages 2331-2341, ISSN 0016-7037

[29] Poppe, A. R., Farrell, W. M., & Halekas, J. S. (2018). Formation timescales of amorphous rims on lunar grains derived from ARTEMIS observations. Journal of Geophysical Research: Planets, 123, 37– 46.

[30] W.M. Farrell, D.M. Hurley, M.I. Zimmerman, Solar wind implantation into lunar regolith: Hydrogen retention in a surface with defects, Icarus, Volume 255,2015, Pages 116-126,ISSN 0019-1035.

[31] Darby Dyar. Darby's glass analytes – June 25, 2012. Darby glass_120313.

[32] Krishnamurthy, R.V. (1998). Hydrogen isotopes. In: Geochemistry. Encyclopedia of Earth Science. Springer, Dordrecht.

[33] J. Phys. Chem. Lett. 2022, 13, 3, 864–871. Publication Date:January 19, 202231] Darby Dyar. Darby's glass analytes – June 25, 2012. Darby glass_120313.

[34] Electron-Stimulated Desorption as a Tool for Studies of Chemisorption: A Review. Theodore E. Madey, John T. Yates. 07 December, 2000. JVST

[35] Wurz, Peter. (2005). Solarwind Composition. 600. 44.

[36] Sulpice, G. Study of the point defects formed in cobalt by electron bombardment; Etude des defauts ponctuels crees par bombardement electronique dans le cobalt. France.

[37] Xiong-Skiba, P., Carroll, D., Doering, D., & Siek, K. (1992). Defects Induced by Electron Bombardment and Substrate Doping in SiO2 Thin Films. MRS Proceedings, 284, 275. doi:10.1557/PROC-284-275

[38] Kuttel, Olivier & Gröning, Pierangelo & Agostino, Raffaele & Schlapbach, Louis. (1995). Mass and energy selected ion beam for deposition and ion induced surface modifications. Journal of Vacuum Science & Technology A: Vacuum, Surfaces, and Films. 13. 2848 - 2855. 10.1116/1.579610.

[39] Ashley R. Clendenen, Aleksandr Aleksandrov, Brant M. Jones, Peter G. Loutzenhiser, Daniel T. Britt, Thomas M. Orlando, Temperature programmed desorption comparison of lunar regolith to lunar regolith simulants LMS-1 and LHS-1, Earth and Planetary Science Letters, Volume 592, 2022, 117632, ISSN 0012-821X.

[40] B.M. Jones, A. Aleksandrov, C.A. Hibbitts, T.M. Orlando. Thermal evolution of water and hydrogen from Apollo lunar regolith grains. Earth Planet. Sci. Lett., 571 (2021)

[41] Hurley, Dana M., Sarantos, Menelaos, Grava, Cesare, Williams, Jean-Pierre, Retherford, Kurt D., Siegler, Matthew, Greenhagen, Benjamin, Paige, David. An analytic function of lunar surface temperature for exospheric modeling. July, 2015. Icarus.

[42] J.P. Pabari, S. Nambiar, V. Shah, Anil Bhardwaj, Lunar regolith and water ice escape due to micrometeorite bombardment, Icarus, Volume 338, 2020, 113510, ISSN 0019-1035.

[43] Zhu, C., Crandall, P. B., Gillis-Davis, J. J., Ishii, H. A., Bradley, J. P., Corley, L. M., & Kaiser, R. I. (2019). Untangling the formation and liberation of water in the lunar regolith. Proceedings of the National Academy of Sciences, 116(23), 11165-11170.

[44] Owens, M.J., & Forsyth, R.J. (2013). The Heliospheric Magnetic Field. Living Reviews in Solar Physics, 10, 1-52.

[45] R.D. Ramsier, J.T. Yates, Electron-stimulated desorption: Principles and applications, Surface Science Reports, Volume 12, Issues 6–8, 1991, Pages 246-378, ISSN 0167-5729.

[46] Thomas M. Orlando, Brant Jones, Carol Paty, Micah J. Schaible, John R. Reynolds, Phillip N. First, Stephen K. Robinson, Valeria La Saponara, Esther Beltran, Catalyst: Radiation Effects on Volatiles and Exploration of Asteroids and the Lunar Surface, Chem, Volume 4, Issue 1, 2018, Pages 8-12, ISSN 2451-9294